Nature of the Bad Metallic Behavior of $Fe_{1.06}Te$ Inferred from Its Evolution in the Magnetic State

Ping-Hui Lin,[1] Y. Texier,[1] A. Taleb-Ibrahimi,[2] P. Le Fèvre,[2] F. Bertran,[2] E. Giannini,[3] M. Grioni,[4] and V. Brouet[1]

[1]*Laboratoire de Physique des Solides, Université Paris—Sud, UMR 8502, Bâtiment 510, 91405 Orsay, France*
[2]*Synchrotron SOLEIL, L'Orme des Merisiers, Saint-Aubin-BP 48, 91192 Gif sur Yvette, France*
[3]*Département de Physique de la Matière Condensée, Université de Genève, 24 Quai Ernest-Ansermet, 1211 Geneva, Switzerland*
[4]*Institut de Physique de la Matière Condensée, Ecole Polytechnique Fédérale de Lausanne, Station 3, CH-1005 Lausanne, Switzerland*

(Received 25 January 2013; published 19 November 2013)

We investigate with angle-resolved photoelectron spectroscopy the changes of the Fermi surface and the main bands from the paramagnetic state to the antiferromagnetic (AFM) state occurring below 72 K in $Fe_{1.06}Te$. The evolution is completely different from that observed in Fe pnictides, as nesting is absent. The AFM state is a rather good metal, in agreement with our magnetic band structure calculation. On the other hand, the paramagnetic state is very anomalous with a large pseudogap of ~65 meV on the electron pocket that closes in the AFM state. We discuss this behavior in connection with spin fluctuations existing above the magnetic transition and the correlations predicted in the spin-freezing regime of the incoherent metallic state.

DOI: 10.1103/PhysRevLett.111.217002 PACS numbers: 74.70.Xa, 71.27.+a, 75.50.Ee, 79.60.−i

An interesting side product of the discovery of Fe-based superconductors (SCs) is the exploration of correlation effects specifically linked to the orbital degeneracy. Hund's couplings may induce new types of correlations. They tend to align spins of the electrons in different orbitals and then favor the formation of local moments which will interact with the itinerant electrons in a Kondo-like fashion [1]. Such a situation may result in very low coherence temperature scales; hence, a large region of "bad metallic behaviors" appears [2]. It was termed a spin-freezing regime [3] because of the presence of these frozen local moments [4,5]. $Fe_{1+y}Te$ (abbreviated as FeTe) clearly qualifies as a "bad metal." Its resistivity increases with decreasing temperature down to the magnetostructural transition $T_{ms} = 72$ K [6]. In the paramagnetic (PM) phase, there is neither evidence for a Drude peak in the optical conductivity nor for a clear gap at low frequencies [6,7]. The susceptibility in the PM state is Curie-like, suggesting localized moments rather than itinerant electrons [6]. In contrast, it is a much better metal in the antiferromagnetic (AFM) state. This difference may help to pinpoint the role of magnetic fluctuations in the bad metallic behavior. Moreover, it places correlation and magnetism at the heart of metallicity in one parent compound of Fe-based SCs.

The relationship between superconductivity and magnetism remains one of the key questions since the discovery of Fe-based SCs [8]. FeTe does not superconduct, but it does when doped with Se (T_c up to 15 K) [9]. It exhibits a double stripe magnetic order [10] [Fig. 1(c)] that contrasts with the stripe order observed in Fe pnictides [8] [Fig. 1(b)]. The associated AFM wave vector $Q_{AFM} = (\pi, 0)$ does not nest the Fermi surface (FS). This rules out the initial idea that magnetism in this family can be described as a simple nesting induced spin density wave. Indeed, the emerging picture is that the magnetic moments are formed due to local interactions on Fe and order in a way that optimizes itinerancy [11]. A dynamic mean field theory (DMFT) approach successfully reproduces experimental values of the magnetic moments and relates them to the strength of correlations [12]. The largest value ($2.2\mu_B$) is found in FeTe, which is also the most correlated case. One qualitative reason is that the Te tetrahedron around the Fe is

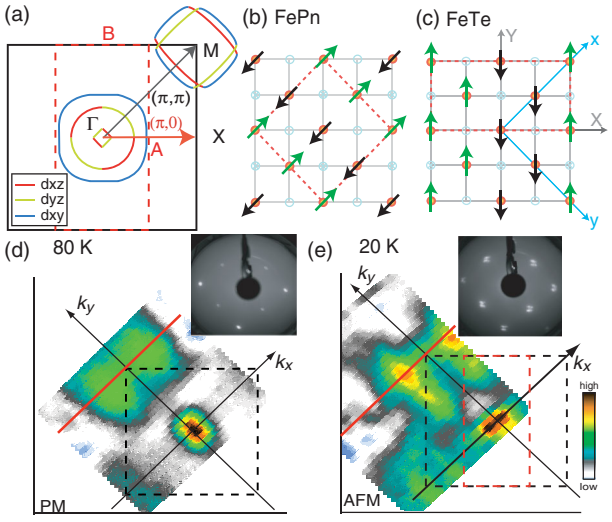

FIG. 1 (color online). (a) Sketch of the PM FS for FeTe. (b) Stripe magnetic order in Fe pnictides $Q_{AFM} = (\pi, \pi)$. (c) Double stripe magnetic order in FeTe $Q_{AFM} = (\pi, 0)$. FS map of FeTe in (d) the PM state (80 K) and (e) the AFM state (20 K). It is obtained by integrating the spectral weight around E_F over ±5 meV, with linear polarization (LP) along k_x and the $h\nu = 70$ eV ($V_0 = 12.5$ eV [14] to correspond to $k_z = 1$). The insets show the LEED at 100 eV of the ab plane in the corresponding state [20]. Dotted red lines in (a) and (e) indicate the AFM BZ.

significantly distorted, pushing Te away from the Fe plane and reducing the overlap between the neighboring Fe [13]. Hence, FeTe provides an opportunity to study magnetism in a "more localized" limit.

Angle-resolved photoelectron spectroscopy (ARPES) studies of Fe chalcogenides have been mostly focused on $Fe_{1+y}Te_{1-x}Se_x$ [14]. As for FeTe, Xia *et al.* [15] reported early on a FS at 27 K but did not study the transition to the PM state. Quite different spectra, usually much broader, were then reported [16,17]. Through the AFM transition, Zhang *et al.* [16] reported a large transfer of spectral weight and the appearance of a small coherent peak. However, the features were too unclear to address specific changes in band structure. Liu *et al.* discussed a similar "peak-dip-hump" line shape within a polaronic picture [17]. We clarify the connection between the band structure in PM and AFM phases by clearly identifying two hole bands and one electron band. These bands display several changes through the magnetic transition: some bands shift and exhibit larger Fermi velocities (v_F) and/or much clearer Fermi crossings below T_{ms}. These changes are roughly in agreement with our magnetic calculations. More importantly, they reveal a complete loss of intensity at the Fermi level (E_F) at the electron pocket in the PM phase, which recovers in the AFM phase. This gives precise indications on how the metallic state is destroyed in the PM phase.

Single crystals of $Fe_{1+y}Te$ ($y = 0.06$, determined by the Energy Dispersive Spectrometer, EDX) were grown by the Bridgman method [18]. The $T_{ms} = 72$ K was determined by SQUID and transport measurements. ARPES experiments were performed at the CASSIOPEE beam line at the SOLEIL synchrotron, with a Scienta R4000 analyzer. The polarization geometry is the same as in Ref. [19]. The energy and angular resolutions were ~25 meV and 0.2°. Temperature dependent measurements were carried out with both decreasing and increasing temperature, starting with samples cleaved in ultrahigh vacuum at high and low temperatures. Results were found to be reproducible and reversible. The narrow spots observed in LEED [shown as the inset in Fig. 1(d)] demonstrate the good surface quality. At 20 K, the spots split due to the monoclinic twinning in the AFM phase [20,21].

The FSs in Figs. 1(d) and 1(e) evidence significant changes from the PM state to the AFM state. The hole pockets at the Brillouin zone (BZ) center change shape. The electron pockets at the BZ corners M are difficult to see in the PM state but become intense in the AFM state. With the new AFM periodicity (red BZ), replicas of hole and electron pockets are expected along the BZ edges at X. There are such features in our data, but with much weaker intensity and not appearing clearly in the FS (see also Refs. [15,16]).

We first focus on the most dramatic evolution, that of the electron pocket at M. Figures 2(a1)–(a4) show their

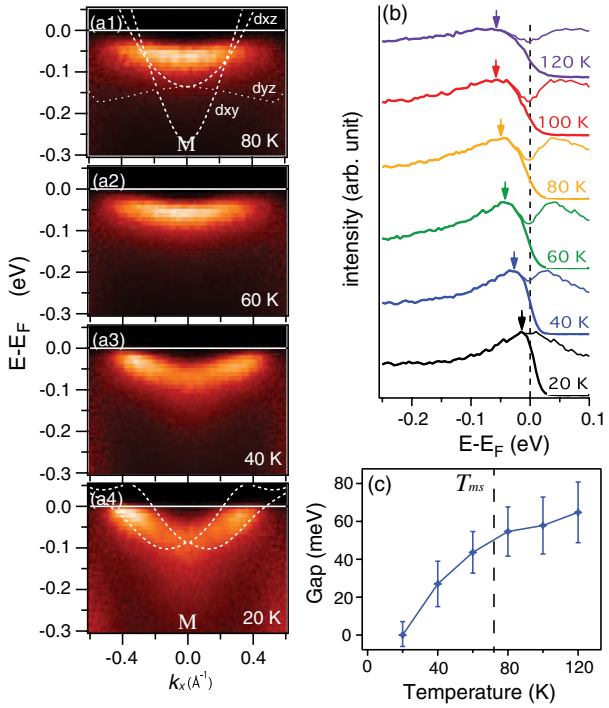

FIG. 2 (color online). (a1)–(a4) Dispersion of the electron pocket in FeTe for the indicated temperatures, along the solid red lines in Figs. 1(d) and 1(e) (parallel to k_x and centered at M). $h\nu = 70$ eV ($k_z \cong 1$) with LP along k_x, which selects orbitals odd/yz. (b) Thick lines: EDCs at k_F for the electron pocket at different temperatures. Thin lines: Symmetrized EDCs. (c) Temperature dependence of the size of PG [arrows in 2(b)].

dispersion measured along the BZ diagonal [red line in Figs. 1(d) and 1(e) [22]] at different temperatures. The dispersion evolves from a nearly flat band at 80 K to a V shaped band at 20 K, with clear Fermi crossings. The corresponding spectra are shown in the Supplemental Material. Figure 2(b) shows the energy distribution curves (EDCs) at k_F, defined as the point where the peak of the EDC is closest to E_F [20]. At 20 K, there is a well defined peak and no gap. As the temperature increases, the peak moves gradually toward higher binding energy and the density at E_F decreases, forming a sort of pseudogap (PG). Symmetrized EDCs, which removes the effect of the Fermi function, are also shown to emphasize the formation of the PG. The dip at E_F indicates the presence of the PG. The peak position indicated by arrows in Fig. 2(b) is reported in Fig. 2(c) as a function of temperature.

Figure 3 further shows the evolution of the hole bands along the BZ diagonal. Two bands are resolved depending on the polarization [19]. For the inner band [Figs. 3(a1)–(a4) and EDC stacks in Ref. [20]], the intensity at 80 K is concentrated at the top of the hole band. When the temperature is lowered, it shifts down by ~80 meV, as detailed in Fig. 3(a5), revealing a small electron pocket on top of it. This brings strong intensity in the FS along that direction, explaining the apparent

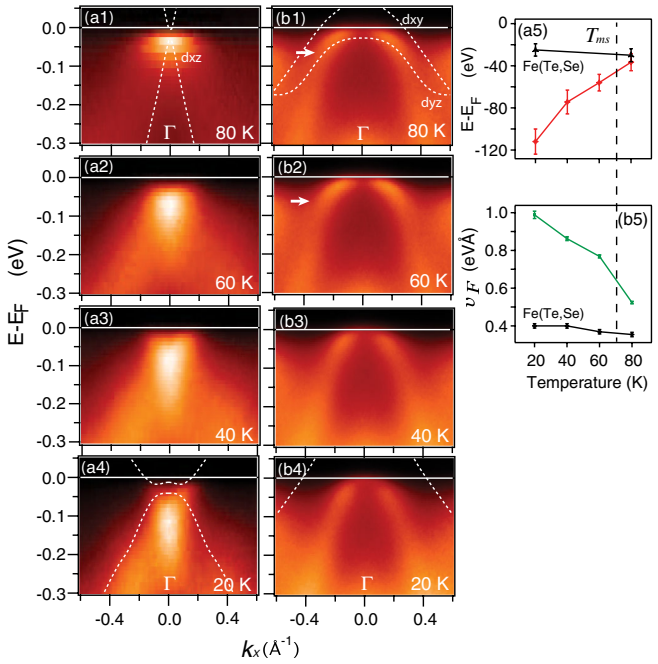

FIG. 3 (color online). (a1)–(a4) Dispersion of FeTe hole pockets at the BZ center for the indicated temperatures. $h\nu = 38$ eV ($k_z \cong 1$) along k_x with (a) LP along k_x, selecting orbitals odd/xz, and (b) LP in the yz plane (even/yz). White arrows indicate the positions of the kinks. (a5) Temperature dependence of the top of the inner hole band in (a1)–(a4). (b5) Temperature dependence of v_F for the outer hole band in (b1)–(b4). The same quantities for $Fe_{1.09}Te_{0.78}Se_{0.22}$ are plotted for comparison.

rotation of the hole pocket in the FS of Fig. 1. The same shift is reported in Ref. [17], along with the appearance of a sharp peak at E_F that is not as clear in our data, maybe due to slightly lower energy resolution. The outer hole band [Figs. 3(b1)–(b4) and Ref. [20]] does not shift as dramatically, but its shape near E_F changes. At high T, a strong kink is observed near ~60 meV, which progressively disappears as temperature decreases. The change of v_F is summarized in Fig. 3(b5). In Figs. 3(a5) and (b5), we show that the values in the PM phase are comparable with those of $Fe_{1.09}Te_{0.78}Se_{0.22}$ [20], where there is no magnetic transition or evolution in this temperature range.

These results suggest a bad metallic behavior for the PM state: the d_{xz}/d_{yz} hole pockets are very small, the d_{xy} hole pocket is not observed and possibly completely incoherent, and the electron pocket is largely gapped. The fact that the coherence of the large electron pocket is recovered in the AFM state proves that the loss of spectral weight is an intrinsic feature of the PM state. Indeed, our observations correlate well with transport measurements in FeTe. In contrast with $BaFe_2As_2$, the Hall coefficient R_H remains large in the AFM state of FeTe [6]. This is because the FS of FeTe does not break into small pockets, as it does in $BaFe_2As_2$ due to the nesting induced FS reconstruction. Moreover, in FeTe, R_H changes sign at T_{ms} and becomes negative in the AFM state [6]. Meanwhile, the thermopower becomes much more negative [23]. These observations are consistent with the larger coherence of the main electron pocket and the development of the small electron pocket at Γ.

We note that all the evolution appears progressively rather than suddenly at the transition, which may be surprising for a first order transition. Our temperature dependent LEED measurement (details in Ref. [20]) indicates that the transition occurs similarly at the surface and in the bulk. It may still be that some surface defects alter the way the magnetic moment develops at the surface, as excess Fe does in $Fe_{1+y}Te$ [10,24].

The AFM state of FeTe is unusual, as it is metallic but not driven by nesting. To better apprehend the impact of the magnetic order on the electronic structure, we show in Fig. 4 a density functional theory calculation performed in the PM and AFM states with the WIEN2K package [25]. The calculation converges to a magnetic moment of $2.2\mu_B$ close to the experimental value, in agreement with previous calculations [13]. As expected from the absence of nesting, the bands folded with the AFM periodicity (dotted lines) do not cross the PM bands near E_F. Consequently, the stabilization of the magnetic state is not due to the opening of gaps at E_F, as in the traditional spin density wave picture, but to a complete reorganization of the electronic structure. Figure 4 shows that the hole d_{xz}/d_{yz} bands shift below E_F by 200 meV for orbitals aligned with the ferromagnetic direction [Y in Fig. 1(c)] and 450 meV for those aligned in the AFM direction [X in Fig. 1(c)]. These different shifts emphasize the differentiation of the two directions in the magnetic state. The bands remaining at E_F are completely rehybridized to optimize new conduction channels along the ferromagnetic direction. Except for a small electron pocket near Γ, no band crosses E_F in the AFM direction. This explains the anisotropy detected recently in detwinned crystals [26].

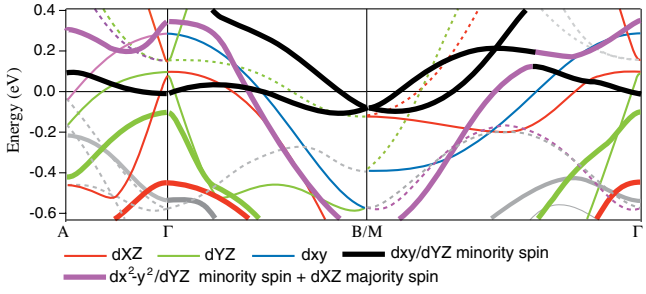

FIG. 4 (color online). Calculated band structure along the AFM (ΓA), ferromagnetic (ΓB), and diagonal (ΓM) directions [Fig. 1(a)]. Thin lines: Bands in the PM state. Dotted lines: Bands folded with respect to the AFM BZ boundaries. Thick lines: Bands in the AFM state. The color indicates the dominant orbital character. d_{XZ} and d_{YZ} are defined in axis, corresponding to the AFM order [Fig. 1(c)].

To compare with this model, we overlay in Figs. 2 and 3 the calculated bands allowed for the given polarization at 20 and 80 K. The calculation is shifted down by 30 meV for the electron band and 120 meV for the hole bands and then renormalized by a factor 2. The shrinking of the d_{xz}/d_{yz} hole pockets is predicted by DMFT [12] and also observed in other systems like LiFeAs [27]. It may be compensated by an expansion of the d_{xy} hole band, but, as we do not observe this band [see Fig. 3(b)], we cannot conclude on this point. The down-shift of the inner hole band and the appearance of the small electron band on top of it in Fig. 3(a) are consistent with the magnetic calculation. In Fig. 3(b1), we only observe the d_{yz} hole band. In the AFM state, the remaining hole band has a much larger k_F in the calculation than in the measurement. We speculate that the rehybridization may take place differently, precisely because d_{xy} and d_{xz}/d_{yz} are not correlated in the same way in the PM state [12], as favored by orbital selective transition scenarios [2,12]. By analogy with Fe pnictides, we presume that the electron band in Fig. 2(a1) is the d_{xz} band, where it strongly dominates in intensity over the d_{xy} band [19]. Of course, the calculation cannot describe the formation of the PG on this band. There are two shallow electron bands at M in the AFM state that are in fact strongly rehybridized compared to the PM state. While we do not have proof for such a rehybridization experimentally, the positions of the pockets themselves are compatible with our ARPES measurement.

The comparison with theory helps to identify the various bands, but the main changes, especially the PG formation, are clearly due to correlations that are extremely sensitive to the magnetic ordering. Our study pinpoints the PG on the electron pocket, which has not been resolved, as the origin of the bad metallic state in FeTe. Strong band renormalization [12] and power law behavior of the imaginary part of the self-energy [4] are expected to characterize the ''spin-freezing'' regime [3]. Here, we use a modest value of renormalization of order 2 to compare experiment and calculation. However, this value is adjusted for a relatively large energy window and would not describe correctly a frequency dependent interaction. At least for the electron pocket, where no quasiparticles (QP) are defined near E_F, speaking of renormalization is not meaningful anymore. Such a loss of intensity through broadening and/or transfer of weight to incoherent structures is expected in a bad metal. What is new in our findings is that the wipeout of the QP occurs in a well defined energy window (~ 60 meV, while the band bottom is broad but still well defined). In addition, it is k dependent, as the intensity near E_F is better defined near Γ than M. However, the 60 meV energy window of the QP wipeout is similar to that of the kink in the outer hole band and also the dip in the peak-dip-hump structure of Ref. [17]. This suggests that the other bands also couple to the same excitations, albeit less strongly. The meaning of this energy scale is an interesting issue. Liebsch suggested that collective spin excitations arising from strong Hund's couplings should result in a PG in the density of states [3]. It would be interesting to investigate further how they would couple to the different bands and change in k space.

In the bad metallic state, DMFT studies predict orbital selective correlations, depending on the effective filling of the orbitals [2,12]. In these scenarios, d_{xy} is found to be more incoherent than d_{xz}/d_{yz}. This could explain why d_{xy} is not observed in our data, neither for hole nor electron pockets. We caution that the d_{xy} band is, however, generally more difficult to see by ARPES in these systems [14,19], making it difficult to be affirmative on this point. One would expect orbital fluctuations to depend on the nesting between the different pockets. A natural wave vector to consider is the one of spin fluctuations. It is known that despite the different $Q_{\mathrm{AFM}} = (\pi, 0)$, magnetic fluctuations are present at (π, π) in the PM state of FeTe and increase with Se doping [28,29]. The electron pocket in FeTe is large and does not nest well with the tiny d_{xz}/d_{yz} hole pockets but possibly better with the incoherent d_{xy} hole pocket, if present [see Fig. 1(a)]. This could explain the preferential appearance of a PG on the electron pocket and reveal important underlying fluctuations between the incoherent d_{xy} and d_{xz}/d_{yz}, mediated by (π, π) spin fluctuations. These fluctuations would vanish in the magnetic state of FeTe ordered at $(\pi, 0)$, which is consistent with the disappearance of the PG.

In conclusion, we have isolated the main bands of FeTe and studied their evolution from the PM to AFM state. Their behavior explains very well the changes observed in transport measurements. The magnetic state is a good metal, while the PM state is a bad metal that deviates strongly from the band calculation. We observe a strong loss of weight near E_F, especially for the electron pockets, where a 65 meV PG opens. Our data support the spin-freezing scenario, as most signs of correlations disappear in the magnetically ordered state. They suggest that a PG results from this spin-freezing regime, which may stimulate more theoretical work. Moreover, they show that different bands couple differently to these excitations, which could be due to underlying orbital fluctuations with a very incoherent d_{xy} band. Recently, a small PG of 20 meV has been reported in K-doped $BaFe_2As_2$ by Xu *et al.* [30]. It is said to coexist with the superconducting gap, persist above T_c up to about 120 K, and be sensitive to the nesting at (π, π). These two situations are quite different, both in ground states and PG strength, but could reveal some universal characteristics of interactions in these systems.

We thank S. Biermann, L. de'Medici, and I. Paul for useful discussion and L. Petaccia for LEED and preliminary ARPES measurements on the BadElph beam line at ELETTRA. Financial support from the ANR Pnictides is acknowledged.

[1] K. Haule and G. Kotliar, New J. Phys. **11**, 025021 (2009).

[2] L. de'Medici, J. Mravlje, and A. Georges, Phys. Rev. Lett. **107**, 256401 (2011).

[3] A. Liebsch, Phys. Rev. B **84**, 180505 (2011).

[4] P. Werner, E. Gull, M. Troyer, and A. J. Millis, Phys. Rev. Lett. **101**, 166405 (2008).

[5] M. Aichhorn, S. Biermann, T. Miyake, A. Georges, and M. Imada, Phys. Rev. B **82**, 064504 (2010).

[6] G. F. Chen, Z. G. Chen, J. Dong, W. Z. Hu, G. Li, X. D. Zhang, P. Zheng, J. L. Luo, and N. L. Wang, Phys. Rev. B **79**, 140509 (2009).

[7] J. N. Hancock, S. I. Mirzaei, J. Gillett, S. E. Sebastian, J. Teyssier, R. Viennois, E. Giannini, and D. van der Marel, Phys. Rev. B **82**, 014523 (2010).

[8] J. Paglione and R. L. Greene, Nat. Phys. **6**, 645 (2010).

[9] P. L. Paulose, C. S. Yadav, and K. M. Subhedar, Europhys. Lett. **90**, 27 011 (2010).

[10] W. Bao, Y. Qiu, Q. Huang, M. A. Green, P. Zajdel, M. R. Fitzsimmons, M. Zhernenkov, S. Chang, M. Fang, B. Qian, E. K. Vehstedt, J. Yang, H. M. Pham, L. Spinu, and Z. Q. Mao, Phys. Rev. Lett. **102**, 247001 (2009).

[11] M. D. Johannes and I. I. Mazin, Phys. Rev. B **79**, 220510 (2009).

[12] Z. P. Yin, K. Haule, and G. Kotliar, Nat. Mater. **10**, 932 (2011).

[13] F. Ma, W. Ji, J. Hu, Z.-Y. Lu, and T. Xiang, Phys. Rev. Lett. **102**, 177003 (2009).

[14] A. Tamai, A. Y. Ganin, E. Rozbicki, J. Bacsa, W. Meevasana, P. D. C. King, M. Caffio, R. Schaub, S. Margadonna, K. Prassides, M. J. Rosseinsky, and F. Baumberger, Phys. Rev. Lett. **104**, 097002 (2010).

[15] Y. Xia, D. Qian, L. Wray, D. Hsieh, G. F. Chen, J. L. Luo, N. L. Wang, and M. Z. Hasan, Phys. Rev. Lett. **103**, 037002 (2009).

[16] Y. Zhang, F. Chen, C. He, L. X. Yang, B. P. Xie, Y. L. Xie, X. H. Chen, M. Fang, M. Arita, K. Shimada, H. Namatame, M. Taniguchi, J. P. Hu, and D. L. Feng, Phys. Rev. B **82**, 165113 (2010).

[17] Z. K. Liu, R.-H. He, D. H. Lu, M. Yi, Y. L. Chen, M. Hashimoto, R. G. Moore, S.-K. Mo, E. A. Nowadnick, J. Hu, T. J. Liu, Z. Q. Mao, T. P. Devereaux, Z. Hussain, and Z.-X. Shen, Phys. Rev. Lett. **110**, 037003 (2013).

[18] R. Viennois, E. Giannini, D. van der Marel, and R. Cern, J. Solid State Chem. **183**, 769 (2010).

[19] V. Brouet, M. F. Jensen, P.-H. Lin, A. Taleb-Ibrahimi, P. Le Fèvre, F. Bertran, C.-H. Lin, W. Ku, A. Forget, and D. Colson, Phys. Rev. B **86**, 075123 (2012).

[20] See Supplemental Material at http://link.aps.org/supplemental/10.1103/PhysRevLett.111.217002 for more details on the sample characterization and the evolution of each band as a function of temperature.

[21] S. Li, C. de la Cruz, Q. Huang, Y. Chen, J. W. Lynn, J. Hu, Y.-L. Huang, F.-C. Hsu, K.-W. Yeh, M.-K. Wu, and P. Dai, Phys. Rev. B **79**, 054503 (2009).

[22] Note that the twinned domains of our crystal give the same contribution along this diagonal.

[23] I. Pallecchi, G. Lamura, M. Tropeano, M. Putti, R. Viennois, E. Giannini, and D. Van der Marel, Phys. Rev. B **80**, 214511 (2009).

[24] I. A. Zaliznyak, Z. Xu, J. M. Tranquada, G. Gu, A. M. Tsvelik, and M. B. Stone, Phys. Rev. Lett. **107**, 216403 (2011).

[25] P. Blaha, K. Schwarz, G. Madsen, D. Kvasnicka, and J. Luitz, *WIEN2K, An Augmented Plane Wave + Local Orbitals Program for Calculating Crystal Properties* (Technische Universitat Wien, Austria, 2002).

[26] J. Jiang, C. He, Y. Zhang, M. Xu, Q. Q. Ge, Z. R. Ye, F. Chen, B. P. Xie, and D. L. Feng, Phys. Rev. B **88**, 115130 (2013).

[27] S. V. Borisenko, V. B. Zabolotnyy, D. V. Evtushinsky, T. K. Kim, I. V. Morozov, A. N. Yaresko, A. A. Kordyuk, G. Behr, A. Vasiliev, R. Follath, and B. Büchner, Phys. Rev. Lett. **105**, 067002 (2010).

[28] T. J. Liu, J. Hu, B. Qian, D. Fobes, Z. Q. Mao, W. Bao, M. Reehuis, S. A. J. Kimber, K. Proke, S. Matas, D. N. Argyriou, A. Hiess, A. Rotaru, H. Pham, L. Spinu, Y. Qiu, V. Thampy, A. T. Savici, J. A. Rodriguez, and C. Broholm, Nat. Mater. **9**, 716 (2010).

[29] M. D. Lumsden, A. D. Christianson, E. A. Goremychkin, S. E. Nagler, H. A. Mook, M. B. Stone, D. L. Abernathy, T. Guidi, G. J. MacDougall, C. de la Cruz, A. S. Sefat, M. A. McGuire, B. C. Sales, and D. Mandrus, Nat. Phys. **6**, 182 (2010).

[30] Y.-M. Xu, P. Richard, K. Nakayama, T. Kawahara, Y. Sekiba, T. Qian, M. Neupane, S. Souma, T. Sato, T. Takahashi, H.-Q. Luo, H.-H. Wen, G.-F. Chen, N.-L. Wang, Z. Wang, Z. Fang, X. Dai, and H. Ding, Nat. Commun. **2**, 392 (2011).